# Tafel-Volmer Electrode Reactions: The Influence of Electron Transfer Kinetics

Chuhong Lin [a], Christopher Batchelor-McAuley [a], Eduardo Laborda [b], Richard G Compton [a*]

[a] Department of Chemistry, Physical and Theoretical Chemistry Laboratory, University of Oxford, South Parks Road, OX1 3QZ, Oxford, United Kingdom

[b] Departamento de Química Física, Facultad de Química, Universidad de Murcia, 30100, Murcia, Spain

*email: richard.compton@chem.ox.ac.uk

**Abstract**

A typical Tafel-Volmer electrode reaction, embracing a preceding chemisorption step and a following electron transfer, is explored by simulation. Two different electron transfer formalisms, Butler-Volmer and a Marcus-Hush like approach, are utilised in interpreting the potential-dependent kinetics of the electrochemical process. Under non-reversible electron transfer conditions, the steady-state voltammetric response at a microdisk electrode is sensitive to the underlying electron transfer kinetics, such that with weak adsorption conditions, the discrepancies between the two electron-transfer models are more pronounced. At high overpotentials, a non-diffusion limited current may either arise from slow adsorption or be a result of Marcus-Hush type kinetics.

**Keywords:** Tafel-Volmer mechanism; Marcus-Hush model; Butler-Volmer model; Steady-state voltammetry; Hydrogen oxidation reaction.

## 1. Introduction

The Butler-Volmer (BV) equation, although phenomenological in its description of electron transfer, has historically been and continues to be successful in describing a wide variety of electrochemical data[1]. However, significant work has been focused upon both providing a more physically correct description of the interfacial electron transfer process[2-3] and determining experimental conditions under which the Butler-Volmer equation is found to be inadequate in describing the electron transfer process.[4-6]

It was with the publication of Chidsey's work in 1991 that the first direct evidence for the limitations of the Butler-Volmer equation was obtained, highlighting how at high overpotentials the rate of electron transfer is significantly below that predicted by the BV equation[5]. This work utilised a surface bound ferrocene group as the electroactive species. Importantly, it is the use of the such a 'diffusionless' system that facilitated the interrogation of the electron transfer kinetics at potentials significantly away from the formal potential for the redox couple, evidencing the validity of the Marcus-Hush (MH) description of electron transfer kinetics. For an outer-sphere diffusional (solution phase) electrochemical system, evidencing distinctions between models of electron transfer becomes inherently challenging in part due to the rate of electrochemical reaction commonly being under mass-transport (diffusion) control at high overpotentials. Recent advancements in the theory of interfacial electron transfer have demonstrated how, for outer-sphere diffusional redox processes, deviations from Butler-Volmer electron transfer kinetics are predicted to be observable under conditions of extremely high mass-transport.[7] Such conditions may be achievable with the use of an electrode with nanoscopic dimensions, however under most experimental conditions the electrochemical response is found to be relatively insensitive to the mechanism of electron transfer (BV vs MH)[8].

Between the limits of the two above cases (surface bound and outer-sphere diffusional) exists a third class of interfacial electrochemical reactions, inner-sphere heterogeneous electrode reactions.[9] Here for inner-sphere reactions, the electroactive species is present in the solution phase however, electron transfer proceeds via one or more surface adsorbed intermediates. This class of reactions encompasses a diverse range of systems including some of the most technological and industrially relevant[10]. Hence, the question arises: are 'inner-sphere' heterogeneous reactions sensitive to the electron transfer mechanism (for example BV vs MH) and under what conditions can discrepancies between the different models of electron transfer be observed? Addressing these questions presents two significant difficulties, first an appropriate electrochemical mechanism needs to be selected and second the form of the kinetic formalism requires consideration. In terms of the overall operative electrochemical mechanism, a host of possible reaction routes may be considered, however within this work the Tafel-Volmer reaction mechanism[11] is taken as a paradigmatic example of an inner-sphere heterogeneous electrochemical process. This reaction path is one route by which hydrogen may be oxidised on some electrodes[12-13] and so is both a 'simple' example of an inner-sphere heterogeneous reaction and is of further academic interest. The question as to the 'appropriate' form of Marcus-Hush electron transfer model is a far more challenging problem. Specifically, the majority of derivations assume that the distance between the electrode and the redox species is significantly larger than ionic radius of the analyte and does not change during the course of the electron transfer event.[14-15] However, for an ion transfer process this approximation does not hold, consequently, inclusion of the molecule/interface distance into the model results in a potential energy surface over which the reaction must proceed.[16] Calculation of the potential energy surface at a single voltage has been previously achieved, such results usefully gain from a theoretical stand-point insight into the relative catalytic properties of different materials.[17] However, consideration of the

reaction pathway as a function of potential is more challenging due partially to the influence of the distribution of the electrostatic potential in the double layer.

On returning to the question of whether the electrochemical response of an inner-sphere heterogeneous reaction is more or less sensitive to the electron transfer mechanism, within this work the Marcus-Hush model of electron transfer is applied, such that the deviation from the Butler-Volmer equation is suitably described by the model. While being aware of the higher complexity of the theoretical description of electro-adsorption/desorption processes[10], in this paper we aim to examine the impact of the electron transfer kinetics on the voltammetric response in view of the non-diffusion limited currents recently reported for the hydrogen oxidation reaction (HOR) at high overpotentials.[11] As a first approach, an MH-like model will be employed. A potential energy curve method with a single reaction coordinate and a (symmetric) Marcusian description of the energy profile; that is, a quadratic variation of the energy with the reaction coordinate that results in a quadratic relationship between the activation energy and the applied potential. This quadratic relationship is in contrast with the linear dependence predicted by the semiempirical BV model. However, strict physical interpretation of the potential energy curve utilised in this work would require inclusion of an understanding of the influence of the inter analyte/electrode distance upon the reaction coordinate. Therefore, application of the Marcus-Hush model within the Tafel-Volmer electrochemical mechanism provides an objective route by which the sensitivity of this paradigmatic ‘inner-sphere’ reaction pathway towards the electron transfer mechanism can be assessed. From this work it is demonstrated that although the Tafel-Volmer reaction is sensitive to the electron transfer model, i.e. differences between the MH and BV processes are clearly demonstrated, the influence of the electron transfer kinetics on the electrochemical response is not unique and may arise from other kinetic limitations of the reaction.

## 2. Theory and Simulation

In this study, the electrode reaction which includes a preceding adsorption step and a following electron transfer step is taken into consideration. The hydrogen oxidation reaction is utilised as an example to explore this type of inner-sphere electrode reaction. Two electron transfer models, the Butler-Volmer and a Marcus-Hush like approach, are applied in the description of the kinetics of the electron transfer process.

### 2.1. The Tafel-Volmer Mechanism

As demonstrated in previous works[11-13], the hydrogen oxidation reaction (Eq.(1)) on Pt electrodes can be regarded as the combination of a chemical adsorption step (the Tafel reaction, Eq.(2)) and an electron transfer step (the Volmer reaction, Eq.(3)):

$$\mathrm{H_2} \rightleftharpoons 2\mathrm{H^+} + 2\mathrm{e^-} \tag{1}$$

$$\mathrm{H_2} + 2\mathrm{M} \underset{k_\mathrm{d}}{\overset{k_\mathrm{a}}{\rightleftharpoons}} 2\mathrm{H(ads)} \tag{2}$$

$$\mathrm{H(ads)} \underset{k_\mathrm{red}}{\overset{k_\mathrm{ox}}{\rightleftharpoons}} \mathrm{H^+} + \mathrm{e^-} + \mathrm{M} \tag{3}$$

where $\mathrm{H(ads)}$ is an adsorbed hydrogen atom, M is an available adsorption site on the electrode surface, $k_\mathrm{a}$ ( m $\mathrm{s^{-1}}$) and $k_\mathrm{d}$ (mol $\mathrm{m^{-2}}$ $\mathrm{s^{-1}}$) are the adsorption and desorption rate constants for the Tafel reaction (Eq.(2)), $k_\mathrm{ox}$ (mol $\mathrm{m^{-2}}$ $\mathrm{s^{-1}}$) and $k_\mathrm{red}$ (m $\mathrm{s^{-1}}$) are the oxidative and reductive electron transfer rate constants for the Volmer reaction (Eq.(3)).

The values of $k_\mathrm{ox}$ and $k_\mathrm{red}$ are dependent on the applied electrode potential $E$ and the formal potential of the electron transfer step $E_{\mathrm{f,\ H^+/H(ads)}}$, which is not identical with the formal

potential of the whole reaction $E_{\mathrm{f,\ H^+/H_2}}$. From the Gibbs energy balance, $E_{\mathrm{f,\ H^+/H(ads)}}$ can be expressed in terms of $E_{\mathrm{f,\ H^+/H_2}}$ and the adsorption equilibrium constant $K_{\mathrm{ads}}$ (unitless):

$$E_{\mathrm{f,\ H^+/H(ads)}} = E_{\mathrm{f,\ H^+/H_2}} + \frac{RT}{2F}\ln\left(K_{\mathrm{ads}}\right) \tag{4}$$

$$K_{\mathrm{ads}} = \frac{k_{\mathrm{a}} c^{o}}{k_{\mathrm{d}}} \tag{5}$$

where the standard concentration $c^{o} = 1$ mol dm$^{-3}$.

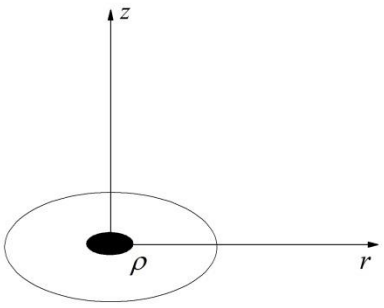


Figure 1 Illustration of the microdisk electrode considered in the simulation. The microdisk electrode (black) is surrounded by an insulating sheath (white). $\rho$ is the radius of the electrode. z and r are the cylindrical coordinates.

According to Eqs.(1), (2) and (3), the fluxes of the electroactive species on the electrode surface can be described as:

$$j_{\mathrm{H_2}}\left(r, z=0, t\right) = -k_{\mathrm{a}} c_{\mathrm{H_2}}(r, z=0, t)\left[\frac{\Gamma_{\mathrm{M}}(r,t)}{\Gamma_{\max}}\right]^2 + k_{\mathrm{d}}\left[\frac{\Gamma_{\mathrm{H(ads)}}(r,t)}{\Gamma_{\max}}\right]^2 \tag{6}$$

$$\frac{\partial \Gamma_{\mathrm{H(ads)}}(r,t)}{\partial t} = 2k_{\mathrm{a}} c_{\mathrm{H_2}}(r,z=0,t)\left[\frac{\Gamma_{\mathrm{M}}(r,t)}{\Gamma_{\max}}\right]^2 - 2k_{\mathrm{d}}\left[\frac{\Gamma_{\mathrm{H(ads)}}(r,t)}{\Gamma_{\max}}\right]^2 - k_{\mathrm{ox}}\left[\frac{\Gamma_{\mathrm{H(ads)}}(r,t)}{\Gamma_{\max}}\right] + k_{\mathrm{red}}\left[\frac{\Gamma_{\mathrm{M}}(r,t)}{\Gamma_{\max}}\right] c_{\mathrm{H^+}}(r,z=0,t) \quad (7)$$

$$j_{\mathrm{H^+}}(r,z=0,t) = k_{\mathrm{ox}}\left[\frac{\Gamma_{\mathrm{H(ads)}}(r,t)}{\Gamma_{\max}}\right] - k_{\mathrm{red}} c_{\mathrm{H^+}}(r,z=0,t)\left[\frac{\Gamma_{\mathrm{M}}(r,t)}{\Gamma_{\max}}\right] \quad (8)$$

$\Gamma_{\mathrm{i}}(r,t)$ is the surface coverage (mol $\mathrm{m^{-2}}$) and $\Gamma_{\mathrm{i}}(r,t)/\Gamma_{\max}$ is the fractional surface coverage (unitless). $\Gamma_{\max}$ is the maximum surface coverage at the electrode surface and $\Gamma_{\max} = \Gamma_{\mathrm{H(ads)}}(r,t) + \Gamma_{\mathrm{M}}(r,t)$. More details about the differences between applying $\Gamma_{\mathrm{i}}(r,t)$ or $\Gamma_{\mathrm{i}}(r,t)/\Gamma_{\max}$ in the rate equations can be found in Supporting Information I. The parameters *r, z* are the cylindrical coordinates used to model a microdisk electrode as shown in Figure 1, and *t* is the time of applying the electrical perturbation. For linear sweep voltammetry, *t* and the applied electrode potential *E* follows:

$$\begin{aligned} &t < t_{\mathrm{switch}}, E = E_{\mathrm{ini}} + vt \\ &t > t_{\mathrm{switch}}, E = E_{\mathrm{switch}} - v(t - t_{\mathrm{switch}}) \end{aligned} \quad (9)$$

where $E_{\mathrm{ini}}$ and $E_{\mathrm{switch}}$ are the initial potential and the switching potential, $t_{\mathrm{switch}}$ is the time at which the direction of sweep is switched, and *v* is the scan rate.

The fluxes in Eqs. (6) and (8) follow the Fick's first law:

$$j_{\mathrm{H_2}}(r,z,t) = -D_{\mathrm{H_2}} \frac{\partial c_{\mathrm{H_2}}(r,z,t)}{\partial z} \quad (10)$$

$$j_{\mathrm{H^+}}(r,z,t) = -D_{\mathrm{H^+}} \frac{\partial c_{\mathrm{H^+}}(r,z,t)}{\partial z} \quad (11)$$

Adsorption is considered to follow a Langmuir isotherm. Thus, the initial surface coverage fractions ( $\Gamma_i(r,t=0)/\Gamma_{max}$ ) for H(ads) and M are:

$$\frac{\Gamma_{H(ads)}(r,t=0)}{\Gamma_{max}} = \frac{\sqrt{c^*_{H_2} k_a / k_d}}{1+\sqrt{c^*_{H_2} k_a / k_d}} \tag{12}$$

$$\frac{\Gamma_{M}(r,t=0)}{\Gamma_{max}} = \frac{1}{1+\sqrt{c^*_{H_2} k_a / k_d}} \tag{13}$$

where $c^*_{H_2}$ is the bulk concentration of the hydrogen molecule.

In addition to the reaction on the electrode surface, the diffusion process of the reactant $H_2$ and the product $H^+$ are also considered in the simulation. Given the electrode geometry shown in Figure 1, the diffusion equations for solution species can be described as:

$$\frac{\partial c_{H_2}(r,z,t)}{\partial t} = D_{H_2}\left(\frac{\partial^2 c_{H_2}(r,z,t)}{\partial r^2} + \frac{1}{r}\frac{\partial c_{H_2}(r,z,t)}{\partial r} + \frac{\partial^2 c_{H_2}(r,z,t)}{\partial z^2}\right) \tag{14}$$

$$\frac{\partial c_{H^+}(r,z,t)}{\partial t} = D_{H^+}\left(\frac{\partial^2 c_{H^+}(r,z,t)}{\partial r^2} + \frac{1}{r}\frac{\partial c_{H^+}(r,z,t)}{\partial r} + \frac{\partial^2 c_{H^+}(r,z,t)}{\partial z^2}\right) \tag{15}$$

## 2.2. Electron Transfer Theories

In the Butler-Volmer model, $k_{ox}$, $k_{red}$ are dependent on the standard heterogeneous rate constant $k_0$ , the transfer coefficient $\alpha$ or $\beta$ ($\alpha+\beta=1$)[18-19], and the applied potential *E*:

$$k_{ox}^{BV} = k_0 c^o \exp\left(\frac{\beta F}{RT}\left(E - E_{f,\ H^+/H(ads)}\right)\right) \tag{16}$$

$$k_{\text{red}}^{\text{BV}} = k_0 \exp\left( -\frac{\alpha F}{RT}\left( E - E_{\text{f, H}^+/\text{H(ads)}} \right) \right) \tag{17}$$

$E_{\text{f, H}^+/\text{H(ads)}}$ is the formal potential associated with the Volmer reaction (Eq.(3)). $E - E_{\text{f, H}^+/\text{H(ads)}}$ is the overpotential of the electron transfer step, which is different from the overpotential for the whole reaction $E - E_{\text{f, H}^+/\text{H}_2}$. Here notice that Eq. (16) is not the common expression for the oxidative electron transfer rate, which reflects the stoichiometry of the reaction and the different standard states defined for solution species and adsorbates on the left and right sides of the electron transfer reaction (Eq. (3)). More details about the derivation can be found in the Supporting Information II.

In the Marcus-Hush model, for an electrochemical reaction $\text{R} \underset{k_{\text{red}}}{\overset{k_{\text{ox}}}{\rightleftarrows}} \text{P} + e^-$, the expression for a rate constant $k$ is derived from a transition state theory approach: [2, 20-21]

$$k_{\text{ox/red}}^{\text{MH}} = A \exp\left( -\frac{\Delta G_{\text{ox/red}}^*}{k_{\text{B}} T} \right) \tag{18}$$

$$\Delta G_{\text{ox/red}}^* = \frac{\lambda}{4}\left( 1 \mp \frac{e\left( E - E_{\text{f, H}^+/\text{H(ads)}} \right) + \varepsilon}{\lambda} \right)^2 \tag{19}$$

where $A$ is the pre-exponential term, which is assumed to be independent on $E$ and $\varepsilon$. $\Delta G_{\text{ox/red}}^*$ (eV) is the activation energy for the oxidative (-) or the reductive (+) process of the electrochemical reaction. $\varepsilon$ (eV) is the energy level of the metal electrode. $\lambda$ (eV) is the reorganization energy. It is worth noting that, within the present context, the "reorganization energy" $\lambda$ has a parametric character, its value being related to the curvature/shape of the energy profile with the reaction coordinate. Thus, in this case the physical meaning of $\lambda$ is likely not only associated with the reorganization of the configuration of the electroactive

species and the solvation shell (as for outer-sphere processes), but also with interactions with the electrode, (partial) desolvation and coulombic forces that the molecule undergoes along the reaction pathway.[10]

For the electron transfer between a reactant and a metal electrode, as there is not a single energy level but an energy band for the metal electrode, the overall rate constant should be the sum of all energy levels, that is $k = \sum k(\varepsilon)$ . Since there are only small intervals $k_B T$ among these energy levels, the probability of this transfer varies very little over two nearby different energy levels in the metal electrode. Therefore, the rate constant expression can be written as[5]:

$$k_{ox}^{MH} = A\int_{-\infty}^{+\infty} \frac{1}{1+\exp\left(\varepsilon^*\right)} \exp\left(-\frac{\lambda^*}{4}\left(1-\frac{\left(E-E_{f,\ H^+/H(ads)}\right)^* + \varepsilon^*}{2\lambda^*}\right)^2\right) d\varepsilon^* \tag{20}$$

$$k_{red}^{MH} = A\int_{-\infty}^{+\infty} \frac{1}{1+\exp\left(-\varepsilon^*\right)} \exp\left(-\frac{\lambda^*}{4}\left(1+\frac{\left(E-E_{f,\ H^+/H(ads)}\right)^* + \varepsilon^*}{2\lambda^*}\right)^2\right) d\varepsilon^* \tag{21}$$

where $f_{ox/red}\left(\varepsilon^*\right) = \frac{1}{1+\exp\left(\pm\varepsilon^*\right)}$ is the Fermi-Dirac distribution for the electron occupancy (+) or the vacancy (-). For convenience, the dimensionless parameters are applied in Eqs. (18) and (19):

$$\lambda^* = \lambda F / (RT) \tag{22}$$

$$\varepsilon^* = \varepsilon F / (RT) \tag{23}$$

$$\left(E-E_{f,\ H^+/H(ads)}\right)^* = \left(E-E_{f,\ H^+/H(ads)}\right) F / (RT) \tag{24}$$

Considering $k_0$ is the standard rate constant at the formal potential, for the Volmer reaction, the MH rate constants can be expressed in a more general way[7]:

$$k_{\mathrm{ox}}^{\mathrm{MH}} = k_0 c^o \frac{\int_{-\infty}^{+\infty} \frac{1}{1+\exp\left(\varepsilon^*\right)} \exp\left( -\frac{\lambda^*}{4}\left( 1-\frac{\left(E-E_{\mathrm{f,\ H^+/H(ads)}}\right)^* + \varepsilon^*}{2}\right)^2\right) d\varepsilon^*}{\int_{-\infty}^{+\infty} \frac{1}{1+\exp\left(\varepsilon^*\right)} \exp\left( -\frac{\lambda^*}{4}\left( 1-\frac{\varepsilon^*}{2}\right)^2\right) d\varepsilon^*} \tag{25}$$

$$k_{\mathrm{red}}^{\mathrm{MH}} = k_0 \frac{\int_{-\infty}^{+\infty} \frac{1}{1+\exp\left(-\varepsilon^*\right)} \exp\left( -\frac{\lambda^*}{4}\left( 1+\frac{\left(E-E_{\mathrm{f,\ H^+/H(ads)}}\right)^* + \varepsilon^*}{2}\right)^2\right) d\varepsilon^*}{\int_{-\infty}^{+\infty} \frac{1}{1+\exp\left(-\varepsilon^*\right)} \exp\left( -\frac{\lambda^*}{4}\left( 1+\frac{\varepsilon^*}{2}\right)^2\right) d\varepsilon^*} \tag{26}$$

Similar to $k_{\mathrm{ox}}^{\mathrm{BV}}$, $k_0$ has been replaced by $k_0 c^0$ in the expression of $k_{\mathrm{ox}}^{\mathrm{MH}}$ .

## 2.3. Numerical simulation

Dimensionless parameters are applied in the simulation, as listed in Table 1. Under the dimensionless format, the diffusion equations for the reactive species in the solution can be described as:

$$\frac{\partial C_{\mathrm{H_2}}\left(R,Z,T\right)}{\partial T} = d_{\mathrm{H_2}}\left( \frac{\partial^2 C_{\mathrm{H_2}}\left(R,Z,T\right)}{\partial R^2} + \frac{1}{R}\frac{\partial C_{\mathrm{H_2}}\left(R,Z,T\right)}{\partial R} + \frac{\partial^2 C_{\mathrm{H_2}}\left(R,Z,T\right)}{\partial Z^2}\right) \tag{27}$$

$$\frac{\partial C_{\mathrm{H^+}}\left(R,Z,T\right)}{\partial T} = d_{\mathrm{H^+}}\left( \frac{\partial^2 C_{\mathrm{H^+}}\left(R,Z,T\right)}{\partial R^2} + \frac{1}{R}\frac{\partial C_{\mathrm{H^+}}\left(R,Z,T\right)}{\partial R} + \frac{\partial^2 C_{\mathrm{H^+}}\left(R,Z,T\right)}{\partial Z^2}\right) \tag{28}$$

The dimensionless boundary conditions for solving diffusion equations can be expressed as:

$$\left.\begin{array}{l} T=0, \forall R, Z \\ T>0, R, Z \to \infty \end{array}\right\} \quad C_{\mathrm{H_2}} = C^{*}_{\mathrm{H_2}} = 1\,, \quad C_{\mathrm{H^+}} = C^{*}_{\mathrm{H^+}} = 0 \tag{29}$$

$$T=0,\ Z=0,\ 0 \le R \le 1: \quad \Theta_{\mathrm{H(ads)}} = \frac{\sqrt{K_\mathrm{a} / K_\mathrm{d}}}{1+\sqrt{K_\mathrm{a} / K_\mathrm{d}}} \tag{30}$$

$T>0,\ Z=0,\ 0 \le R \le 1$:

$$-d_{\mathrm{H_2}} \left(\frac{\partial C_{\mathrm{H_2}}}{\partial Z}\right)_{Z=0} = K_\mathrm{d} \Theta^2_{\mathrm{H\,(ads)}} - K_\mathrm{a} \left(1-\Theta_{\mathrm{H\,(ads)}}\right)^2 C_{\mathrm{H_2}} \tag{31}$$

$$-\mathrm{d}_{\mathrm{H^+}} \left(\frac{\partial C_{\mathrm{H^+}}}{\partial Z}\right)_{Z=0} = K_{\mathrm{ox}} \Theta_{\mathrm{H\,(ads)}} - K_{\mathrm{red}} \left(1-\Theta_{\mathrm{H\,(ads)}}\right) C_{\mathrm{H^+}} \tag{32}$$

$$\begin{aligned} \left(\frac{\partial \Theta_{\mathrm{H\,(ads)}}}{\partial T}\right) &= 2K_\mathrm{a} \gamma \left(1-\Theta_{\mathrm{H\,(ads)}}\right)^2 C_{\mathrm{H_2}} - 2K_\mathrm{d} \gamma \Theta^2_{\mathrm{H\,(ads)}} \\ &\quad + K_{\mathrm{red}} \gamma \left(1-\Theta_{\mathrm{H\,(ads)}}\right) C_{\mathrm{H^+}} - K_{\mathrm{ox}} \gamma \Theta_{\mathrm{H\,(ads)}} \end{aligned} \tag{33}$$

$T>0,\ Z=0,\ R>1$:

$$\left(\frac{\partial C_{\mathrm{H_2}}}{\partial Z}\right)_{Z=0} = 0 \ ; \quad \left(\frac{\partial C_{\mathrm{H^+}}}{\partial Z}\right)_{Z=0} = 0 \tag{34}$$

$T>0,\ Z,\ R=0$:

$$\left(\frac{\partial C_{\mathrm{H_2}}}{\partial R}\right)_{R=0} = 0 \ ; \quad \left(\frac{\partial C_{\mathrm{H^+}}}{\partial R}\right)_{R=0} = 0 \tag{35}$$

where the parameter $\gamma$ is generated from the dimensionless process, equal to $\frac{c^{*}_{\mathrm{H_2}} \rho}{\Gamma_{\max}}$. From Table 1, it is found that $\gamma$ is the only constant parameter that contains $\Gamma_{\max}$ ($\Theta_\mathrm{i} = \Gamma_\mathrm{i} / \Gamma_{\max}$ works as a variable not a constant parameter during the simulation). Under steady state conditions, as $\partial \Theta_{\mathrm{H\,(ads)}} / \partial T = 0$, parameter $\gamma$ cancels out in Eq. (33) such that the response of the system is independent of its value. It also indicates that for transient voltammetry where $\partial \Theta_{\mathrm{H\,(ads)}} / \partial T \neq 0$, the value of $\gamma$ cannot be cancelled out from Eq. (33) and consequently the voltammogram will be influenced by the magnitude of $\Gamma_{\max}$.

The resulting problem was solved numerically by means of the Newton-Raphson method and according to the alternating direction implicit (ADI) method, the details of which can be found in the textbook[22]. The simulation was written in C++ with OpenMP for multithreading and simulations were performed using an Intel(R) Xeon(R) 3.60G CPU and the runtime was approximately 10 minutes *per* voltammogram.

Table 1 Dimensionless parameters employed in the simulations

| SI unit parameters | Dimensionless parameters |
|---|---|
| $c_{\mathrm{j}}$ | $C_{\mathrm{j}} = c_{\mathrm{j}} / c^{*}_{\mathrm{H_2}}$ |
| $\Gamma_{\mathrm{i}} / \Gamma_{\max}$ | $\Theta_{\mathrm{i}} = \Gamma_{\mathrm{i}} / \Gamma_{\max}$ |
| $D_{\mathrm{j}}$ | $d_{\mathrm{j}} = D_{\mathrm{j}} / D_{\mathrm{H_2}}$ |
| $r$ | $R = r / \rho$ |
| $z$ | $Z = z / \rho$ |
| $t$ | $T = D_{\mathrm{H_2}} t / \rho^2$ |
| $E$ | $\theta = (F / RT)(E - E_{\mathrm{f,\ H^+/H_2}})$ |
| $E_{\mathrm{f,\ H^+/H(ads)}}$ | $\theta_{\mathrm{f,\ H^+/H(ads)}} = (F / RT)(E_{\mathrm{f,\ H^+/H(ads)}} - E_{\mathrm{f,\ H^+/H_2}})$ |
| $\nu$ | $\sigma = (\rho^2 / D_{\mathrm{H_2}})(F / RT)\nu$ |
| $I$ | $J = I / (2\pi\rho F D_{\mathrm{H_2}} c^{*}_{\mathrm{H_2}})$ |
| $k_{\mathrm{a}}$ | $K_{\mathrm{a}} = k_{\mathrm{a}}\rho / D_{\mathrm{H_2}}$ |
| $k_{\mathrm{d}}$ | $K_{\mathrm{d}} = k_{\mathrm{d}}\rho / \left(D_{\mathrm{H_2}} c^{*}_{\mathrm{H_2}}\right)$ |
| $K_{\mathrm{ads}} = k_{\mathrm{a}} c^{o} / k_{\mathrm{d}}$ | $K_{\mathrm{ads}} = K_{\mathrm{a}} c^{o} / \left(K_{\mathrm{d}} c^{*}_{\mathrm{H_2}}\right)$ |
| $k_0$ | $K_0 = k_0\rho / D_{\mathrm{H_2}}$ |
| $k_{\mathrm{ox}}$ | $K_{\mathrm{ox}} = k_{\mathrm{ox}}\rho / \left(D_{\mathrm{H_2}} c^{*}_{\mathrm{H_2}}\right)$ |
| $k_{\mathrm{red}}$ | $K_{\mathrm{red}} = k_{\mathrm{red}}\rho / D_{\mathrm{H_2}}$ |
| $\lambda^{*}$ | $\lambda F / \left(RT\right)$ |
| $\varepsilon^{*}$ | $\varepsilon F / \left(RT\right)$ |
| | $\gamma = c^{*}_{\mathrm{H_2}}\rho / \Gamma_{\max}$ |

## 3. Results and Discussion

In this section, the empirical Butler-Volmer model of the electron transfer is compared with the Marcus-Hush like model in respect of their effects on the Tafel-Volmer mechanism and associated voltammetry. The steady-state voltammetric responses at microdisk electrodes of the two electron transfer models are examined under different electron transfer kinetics and adsorption behaviours.

### 3.1. Influence of the Electron Transfer Reversibility

Figure 2 shows the variation of the steady-state voltammograms with a series of standard dimensionless heterogeneous rate constants $K_0$. The electron transfer models used in Figure 2a and 2b are described by the BV and the MH formulas, respectively. The value of the adsorption equilibrium constant $K_{ads}$ is always set to unity such that the formal potential of the electron transfer reaction $\theta_{f,\,H^+/H(ads)}$ coincides with the formal potential of the whole hydrogen oxidation reaction $\theta_{f,\,H^+/H_2}$ (Eq.(4)). Also, the adsorption and desorption rate constants $K_a$, $K_d$ are considered to be so fast as not to be the limiting factor of the overall reaction. The value of $K_0$ varies from $10^8$ to $10^{-3}$, covering the transition from electrochemical reversibility to slow ("non-reversible") electron transfer. As expected, the electrochemically reversible reactions (i.e. $K_0 = 10^8$ and $K_0 = 10^3$), the voltammograms obtained with the two kinetic models coincide because they both follow the Nernst equation that along with the diffusive mass transport define the voltammograms. On the other hand, important differences between the BV and MH models are found for electrochemically non-reversible processes. Thus, under the same diffusion conditions, slow electrode kinetics

affects the steady-state voltammogram by increasing the overpotential required to drive the current. Also, a decrease of the limiting current is predicted by the MH formalism.

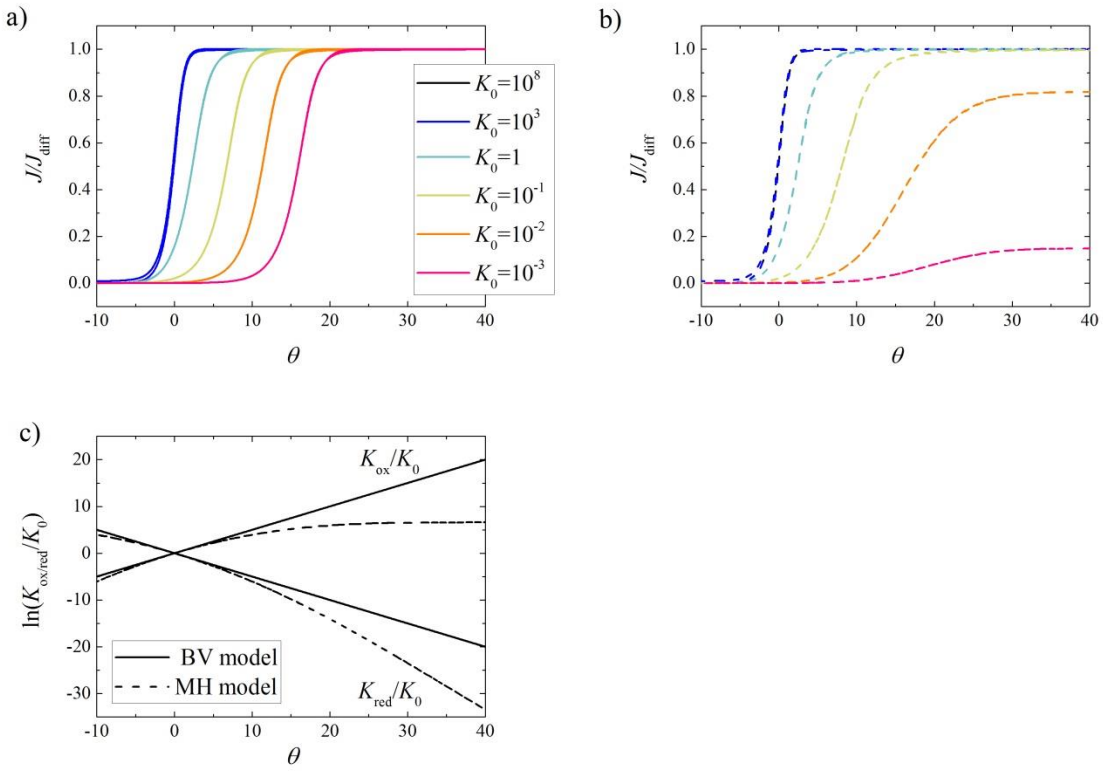


Figure 2 Effects of the dimensionless standard heterogeneous rate constants $K_0$ on the voltammmograms obtained with: a) The Butler-Volmer model; b) The Marcus-Hush model; c) The comparison of the electron transfer constants between the two kinetic models. The dimensionless current is normalized by the diffusion limited current $J_{diff}$ . Simulation parameters for the adsorption step are: $K_a = K_d = 10^8$. In the BV model, $\alpha = \beta = 0.5$; in the MH model, $\lambda^* = 20$. $\theta$ is the dimensionless overpotential for the overall reaction.

In the BV model (Figure 2a), for the reaction with small $K_0$ values, the voltammograms shift to higher overpotentials while the limiting current is the same as the reversible value, which is the diffusion limited current $J_{\text{diff}}$. This is because the electrooxidation rate $K_{\text{ox}}^{\text{BV}}$ increases ad infinitum with overpotential (Figure 2c). Therefore by increasing the overpotential, it is always possible to achieve electron transfer kinetics that is not rate limiting and only a potential shift is observed in the voltammograms. Compared with the BV voltammograms in Figure 2a, the decrease of $K_0$ in the MH model in Figure 2b leads to much more apparent changes. The overall reaction rates under the MH model are obviously slower than those under the BV models as shown in Figure 2c, reflected both in the decline of the limiting current and the increase of the overpotential. This can be explained as a consequence of a limiting electron transfer rate constant at high overpotentials predicted by the MH model. As shown in Figure 2c, these two models predict similar electron transfer rate constants only at the overpotentials near $\theta_{\text{f, H}^+/\text{H(ads)}}$, which is equal to $\theta_{\text{f, H}^+/\text{H}_2}$ in this case. $K_{\text{ox/red}}^{\text{BV}}$ varies exponentially with the overpotential while $K_{\text{ox/red}}^{\text{MH}}$ tends to reach a limiting value at high overpotentials, which kinetically controls the maximum rate of the whole reaction. This trend for the Tafel-Volmer type of reaction is consistent with that reported for a simple outer-sphere one-electron-transfer reaction. [7, 23]

In the MH kinetics, the parameter $\lambda^*$ plays a key role as well. Figure 3 shows the voltammetric responses of a Tafel-Volmer reaction for different $\lambda^*$ values. As shown in Figure 3a, the decrease of $\lambda^*$ leads to the decline in the limiting current. Figure 3b provides details about the electron transfer rates varying with different $\lambda^*$. It is found that the maximum rate constant for the electron transfer step falls with decreasing $\lambda^*$, which explains the voltammograms in Figure 3a.

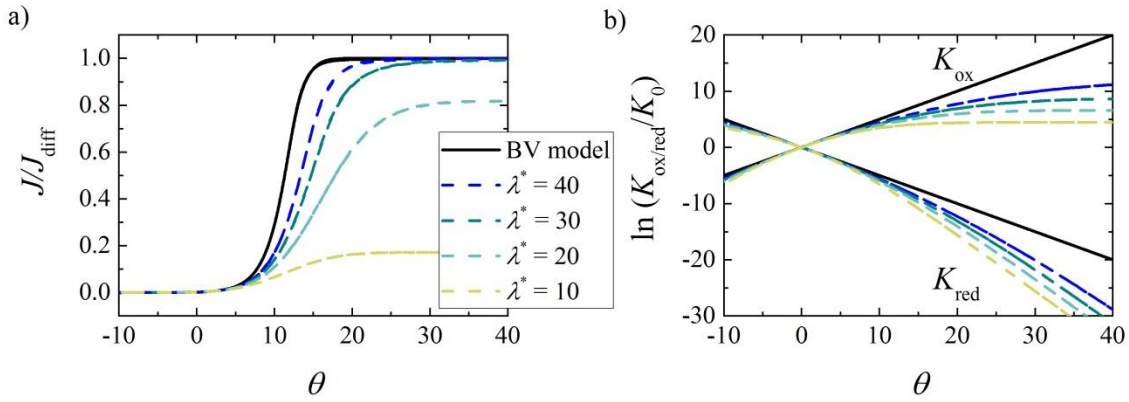


Figure 3 Effects of the "reorganization energy" $\lambda^*$ on: a) Steady-state voltammograms; b) Oxidative and reductive electron transfer rates. Dashed lines correspond to results obtained from the MH model and solid lines are from the BV model. $K_0 = 10^{-2}$ and $K_a = K_d = 10^8$. $\theta$ is the dimensionless overpotential for the overall reaction.

### 3.2. Influence of Adsorption on Reversible Electron Transfer

In this subsection, the influence of adsorption is studied under reversible electron transfer conditions ($K_0 \gg 1$). $K_{ads}$ is not constrained to being unity and $K_a$, $K_d$ changes over a large range. When the electron transfer step is regarded as fast (reversible, $K_0 \gg 1$), the surface concentrations of the reactive species should follow the Nernst equation and hence the BV and MH formulas lead to identical voltammetric responses. The main features of a steady-state voltammogram (that is, the limiting current $J_{lim}$ and the half-wave overpotential $\theta_{1/2}$) are controlled by either the diffusion or the adsorption/desorption rates[11-13, 24]. Figure 4 shows the voltammograms of an electrochemically reversible Tafel-Volmer reaction for different adsorption/desorption rate constants. In Figure 4a, the decrease of $K_d$ shifts the wave to

higher overpotentials. When $K_a$ varies from $10^3$ (shown by the solid lines) to $10^7$ (shown by the open circles), changes in $K_a$ (and so $K_{ads}$) have no influence on the position of the voltammograms. Similarly, in Figure 4b, for $K_d$ equal to $10^7$ (solid lines) and $10^{-1}$ (open circles), the normalized limiting current is only dependent on the value of $K_a$. Under the electrochemically reversible case, the limiting current can be written as a function of the adsorption rate constant $K_a$ (see Appendix III for the derivation and validation check):

$$\frac{J_{lim}}{J_{diff}} = \frac{\frac{\pi}{4}K_a}{1+\frac{\pi}{4}K_a} \tag{36}$$

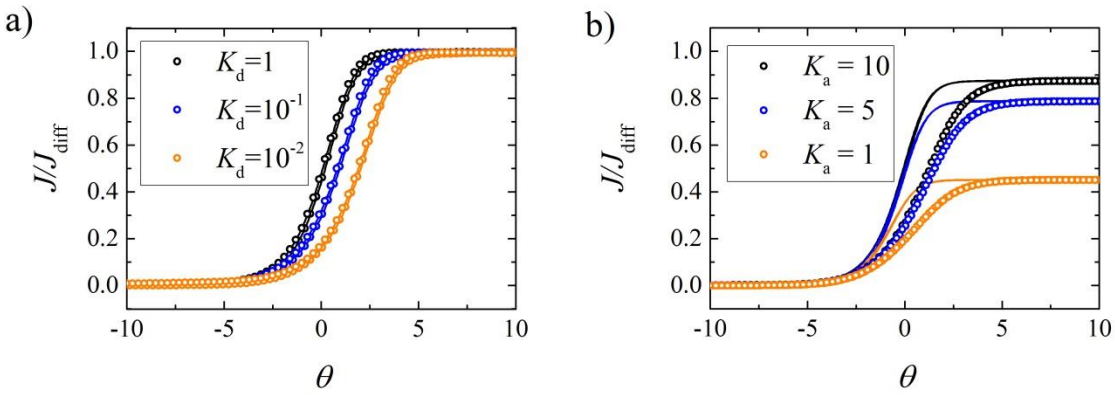


Figure 4 Voltammograms of the electrochemically reversible HOR under different adsorption conditions. a) Half-wave potential shift with decreasing $K_d$ (solid lines: $K_a$ = $10^3$, open circles: $K_a$ = $10^7$); b) Normalized limiting current decline with decreasing $K_a$ (solid lines: $K_d$ = $10^7$, open circles: $K_d$ = $10^{-1}$). $K_0 = 10^8$. $\theta$ is the dimensionless overpotential for the overall reaction.

Figure 5 provides a general view on the change of the normalized limiting current $J_{lim}/J_{diff}$ and the half-wave overpotential $\theta_{1/2}$ under various adsorption/desorption rate constants. From Eq. (36) and Figures 4, 5, it can be seen that for the electrochemically reversible Tafel-Volmer reaction, the normalized limiting current $J_{lim}/J_{diff}$ is only dependent on the value of $K_a$. Figure 5b shows the half-wave overpotential varying with different $K_a$ and $K_d$. In general, based on the thermodynamic arguments, the half-wave overpotential should not be smaller than the reversible value. However, considering that small adsorption rate constants can cause a decrease in the limiting current, this leads to an artificial shift of the half-wave potential. Except for this interference from slow adsorption rate constants, the half-wave potential is mainly determined by the value of $K_d$ rather than $K_{ads}$, indicating that changing the thermodynamics of the preceding adsorption step will not cause any significant differences on the voltammogram for an electrochemically reversible Tafel-Volmer reaction.

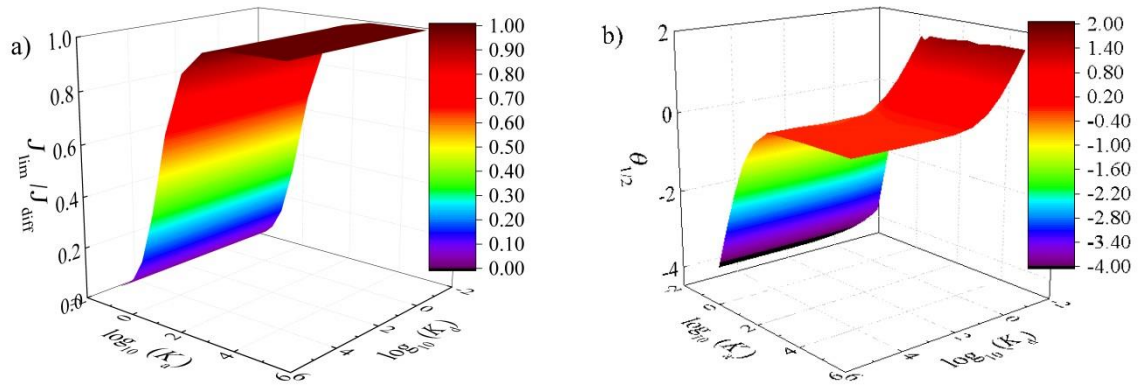


Figure 5 Voltammetric features, a) The normalized limiting current; b) The half-wave overpotential, under different adsorption conditions for reversible electron transfer. The heterogeneous standard rate constant $K_0 = 10^8$. $\theta$ is the dimensionless overpotential for the overall reaction.

3.3. Influence of Adsorption on Non-reversible Electron Transfer

For the electrochemically non-reversible case (small $K_0$), apart from the effects from slow adsorption/desorption kinetics ($K_a$, $K_d$), the whole reaction is expected to be sensitive to the adsorption thermodynamics ($K_{ads}$) as well. Although the formal potential of the electron transfer step $\theta_{f,\ H^+/H(ads)}$ is always dependent on $K_{ads}$, only when $K_0$ is small, is the change of formal potential (and hence the overpotential) expected to have an apparent influence on the overall reaction rate.

Figure 6 shows the effects of the adsorption thermodynamics ($K_{ads}$) on the voltammograms simulated in the BV model (Figure 6a) and the MH model (Figure 6b). In order to distinguish this case from the electrochemically reversible reactions discussed above, the standard heterogeneous constant $K_0$ is selected as $10^{-2}$ and $\lambda^*$ used in the MH model is 20. As shown in Figure 6a, in the BV model, the normalized limiting current is always unity (diffusion controlled) but the overpotential changes with $K_{ads}$. Both strong (large $K_{ads}$) and weak (small $K_{ads}$) chemical adsorptions make the overpotential shift positively. In the MH model, strong adsorption leads to a similar overpotential shift while weak adsorption significantly decreases the limiting current, which is visibly different from that predicted by the BV model (Figure 6a). Here to avoid any additional effect from slow adsorption/desorption, the values of the applied $K_a$ and $K_d$ for Figure 6 are relatively fast, as listed in Supporting Information IV (Table S2). Compared with Figure 5, it is found that these $K_a$, $K_d$ applied in Figure 6 should not lead to any extra potential shift. Therefore, the changes of the waveshape in Figure 6 are only attributed to the value of $K_{ads}$.

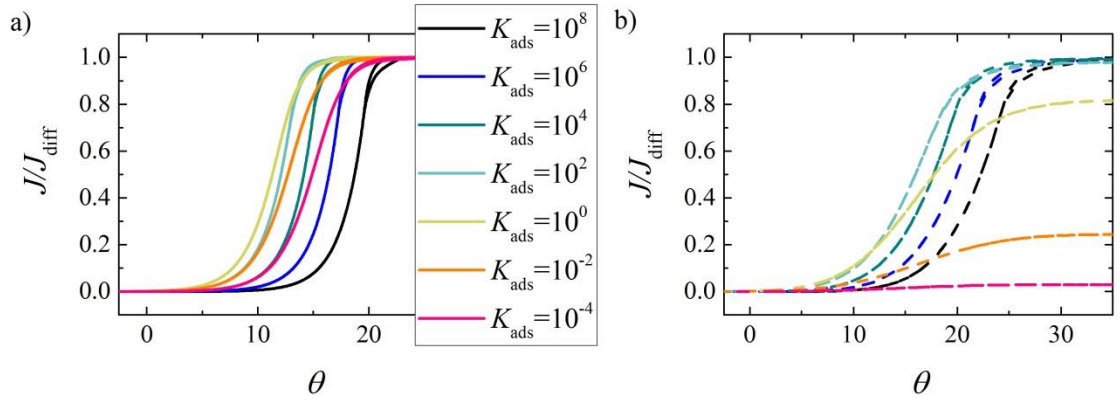


Figure 6 Voltammograms of electrochemically non-reversible Tafel-Volmer reaction with different adsorption conditions. a) Butler-Volmer electron transfer model ($K_0$ = $10^{-2}$ and $\alpha = \beta = 0.5$); b) Marcus-Hush electron transfer model ($K_0$ = $10^{-2}$ and $\lambda^*$ = 20). The parameters of the adsorption step used in the simulation are listed in Table S2. $\theta$ is the dimensionless overpotential for the overall reaction.

Figure 7 provides a general view on the effect of the Tafel step under electrochemically non-reversible conditions, covering the adsorption and desorption rate constants from $10^{-2}$ to $10^{8}$. The results are calculated from the BV model ($K_0$ = $10^{-2}$ and $\alpha$ = $\beta$ = 0.5) and the MH model ($K_0$ = $10^{-2}$ and $\lambda^*$ = 20). Unlike in Figure 6, the additional effect of slow adsorption and desorption is also taken into consideration in Figure 7 where the variation of the normalized limiting current $J_{lim}/J_{diff}$ and the overpotential corresponding to $0.01J_{diff}$ ($\theta_{0.01J_{diff}}$) are studied as the characteristic magnitudes of the voltammetric responses. The reason for the use of $\theta_{0.01J_{diff}}$ rather than $\theta_{1/2}$ in Figure 7 (and also Figure 8) is that when the adsorption thermodynamics effect ($K_{ads}$) on the electron transfer kinetics is explored, the comparison of the overpotential at the same current corresponding to the foot of the wave can clearly reveal

the change of the formal potential of the electron transfer step, without the interference of the adsorption/desorption kinetics discussed in Figure 5. On the other hand, in Figure 5 (and Figure 9 as well), the kinetics of the adsorption step ($K_a$, $K_d$) is explored and its effect on the whole voltammogram, such that the half-wave overpotential is chosen as the measurement of the wave position. From Figure 7a and 7b simulated in the BV model, it can be seen that the limiting current of the BV model is only related to the value of $K_a$, similarly to that observed for reversible electron transfers in Figure 5a. On the other hand, the overpotential shift is not solely determined by $K_d$ but instead mainly dependent on the value of $K_a/K_d$ ($K_{ads}$). Figure 7c and 7d are simulated under the MH model. In contrast to the BV model, the limiting current of the MH model is determined by both $K_a$ and $K_d$ and higher overpotential is needed to obtain the same current in the MH model.

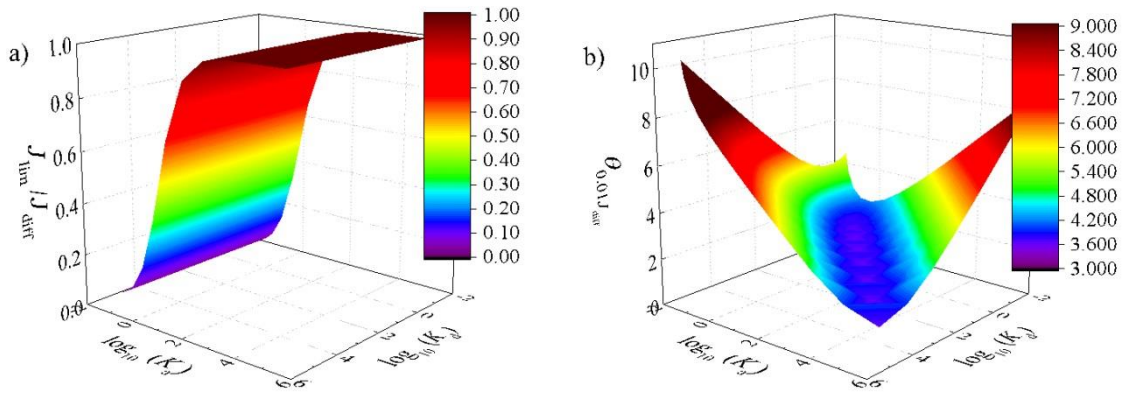

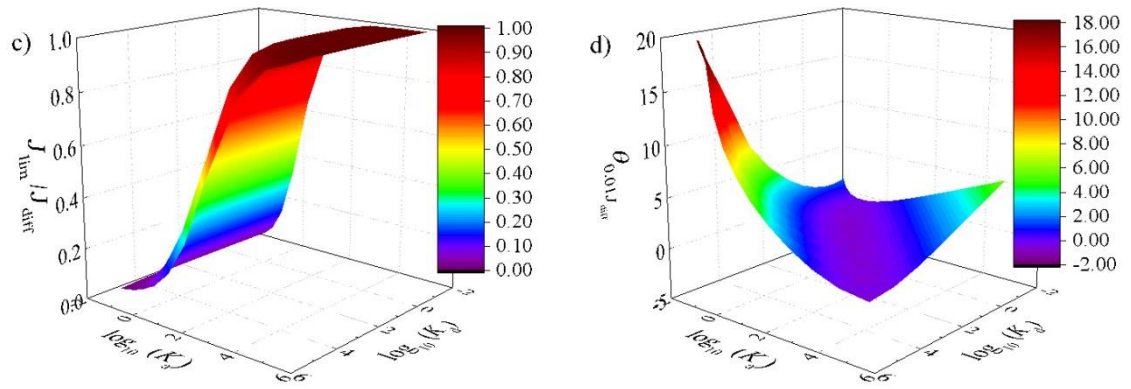


Figure 7 Voltammetric features under different adsorption conditions and electron transfer models for non-reversible electron transfer. a) Normalized limiting current under the BV model; b) The overpotential when $J = 0.01J_{diff}$ under the BV model; c) Normalized limiting current under the MH model; d) The overpotential when $J = 0.01J_{diff}$ under the MH model. For the BV model, $K_0 = 10^{-2}$ and $\alpha = \beta = 0.5$; for the MH model, $K_0 = 10^{-2}$ and $\lambda^* = 20$. $\theta$ is the dimensionless overpotential for the overall reaction.

In both the BV and MH models, when the electron transfer step is not reversible, the value of $\theta_{0.01J_{diff}}$ changes parabolically with $K_{ads}$ (see Figure 7b and 7d), which implies that both strong and weak adsorption can impede the reaction. According to the Sabatier principle[25], optimal electrocatalysis happens when the adsorption is neither strong nor weak. In the Tafel-Volmer mechanism, strong adsorption makes the formal potential for the electron transfer step $\theta_{f,\ H^+/H(ads)}$ move positively and hence the overpotential has to increase in order to drive the electrochemical reaction. Therefore, the voltammetric wave shifts to higher potentials when the interaction between the hydrogen and the electrode is stronger. For weak adsorption, although the electron transfer reaction is more favourable thermodynamically, the

voltammogram also shift to higher overpotentials as a result of the low availability of adsorbed hydrogen on the electrode surface. Moreover, compared with the BV model, in the MH model, the limiting current decreases and higher overpotential is required to obtain the same current, especially under weak adsorption conditions (small $K_a / K_d$). This can be explained as follows: the amount of adsorbed hydrogen becomes insufficient for the Volmer reaction and the lack of H(ads) accentuates the limitation by the electron transfer rate constants $K_{ox}^{MH}$. Interestingly, the BV and MH models give almost the same voltammetric responses when the adsorption is strong (large $K_a / K_d$), indicating that the discrepancies between the two kinetic models can be more clearly observed under weak adsorption conditions whereas strong adsorption can partially compensate the loss of the reaction rate caused by slow electron transfer rate at high overpotentials. Thus, the maximum reaction rate for a Tafel-Volmer reaction is directly linked with the electron transfer rate, given by $K_{ox}\Theta_{H(ads)}$ at high overpotentials. For the Tafel-Volmer reaction with a slow MH electron transfer kinetics, although $K_{ox}$ reaches a limiting value, there are more adsorbed hydrogen atoms on the electrode surface under strong adsorption conditions rather than weak adsorption, as the initial amount of adsorbed hydrogen is determined by $K_{ads}$ (Eq. (30)).

Figure 8 shows the variation of the limiting current and the overpotential corresponding to $0.01J_{diff}$ with the value of $K_{ads}$ for $\lambda^*$ = 10, 20, 30, 40. In Figure 8a, as the applied $K_a$ and $K_d$ are the same as in Figure 6, it is clear that under any adsorption conditions, the values of the limiting current simulated from the BV model are equal to the diffusion limited current. For the MH model, as discussed in Figure 3, the values of the limiting currents calculated from small reorganization energies are much lower than the diffusion limited value. It is also shown in Figure 8a that the decrease of $J_{lim}$ caused by non-reversible electron transfer can be partially compensated by a strong adsorption step. Here the adsorption equilibrium constant

$K_{ads}$ at which the electron transfer limitation of the MH model starts to be detectable is dependent on the reversibility of the electron transfer step. When the electron transfer becomes more irreversible (e.g. small $K_0$ and/or small $\lambda^*$), for the MH model, the deviation from the diffusion limited current can be observed for stronger adsorption.

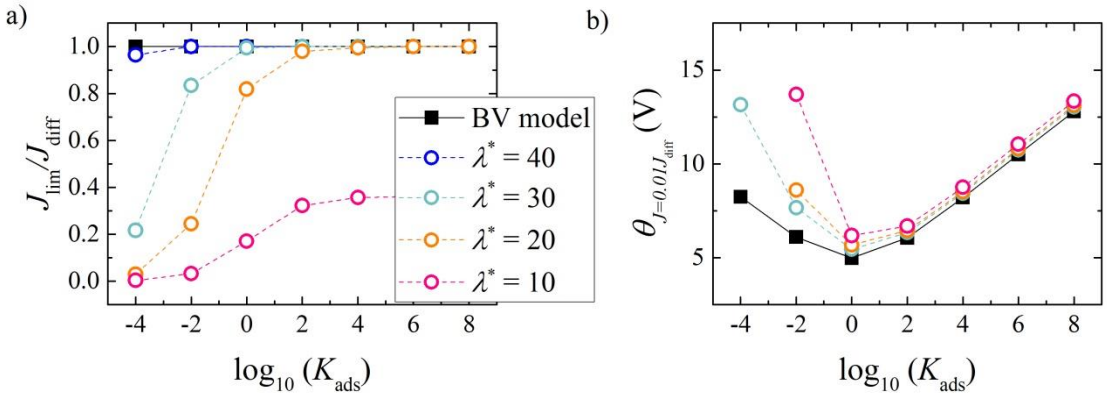


Figure 8 Voltammetric features of electrochemically non-reversible HOR with different adsorption conditions. a) Normalized limiting current; b) Overpotential where $J = 0.01J_{diff}$. $K_a$, $K_d$ are the same as listed in Table S2. $\theta$ is the dimensionless overpotential for the overall reaction.

### 3.4. Influence of Diffusion on Different Limiting Factors

In the BV model, the slow adsorption rate constant (small $K_a$) can determine the maximum current of the whole reaction, while in the MH model, even with fast adsorption (large $K_a$), the reorganization energy has similar effects as shown in Figure 6. Therefore, for the Tafel-Volmer type of reaction, if the limiting current of a steady-state voltammogram is less than the diffusion controlled value, it can be limited by either a slow preceding adsorption or a

sluggish electron transfer step that follows a MH type kinetics. In order to examine if these two limiting factors can be experimentally distinguished, voltammograms for the two situations are simulated under different diffusion conditions. In experiments this corresponds to the use of electrodes of different sizes. In Figure 9, an adsorption limited reaction in the BV model with $K_0 = 10^{-2}$ and $K_a = 60$ and an electron transfer limited reaction in the MH model with $K_0 = 10^{-2}$ and $\lambda^* = 20$ are taken as examples, the variations of $J_{lim} / J_{diff}$ and $\theta_{1/2}$ with the radius of the electrode being explored. Note that to clearly show the results, the real radius with units of $\mu$m is considered. Other parameters are still dimensionless to remain consistent with other figures. At "large" microdisk electrodes (i.e., $\rho$ = 50.0 $\mu$m), due to the relatively slow diffusion, the reaction rate is controlled by mass transport and the two limiting factors above mentioned have little discrepancies in the voltammetric features. With the decrease of the electrode size, diffusion becomes more efficient and the limiting factors have different behaviours: The limiting current decreases faster in the MH model (electron transfer controlled) than in the BV model (adsorption controlled) and the half-wave overpotential shifts more positively for the MH model as well. However, the general trends of their responses to the diffusion change are the same for limitations associated with both adsorption and electron transfer kinetics. Thus, when the reaction is not electrochemically reversible, it is difficult to determine if the decrease of the limiting current is caused by a slow adsorption step or a sluggish MH electron transfer step.

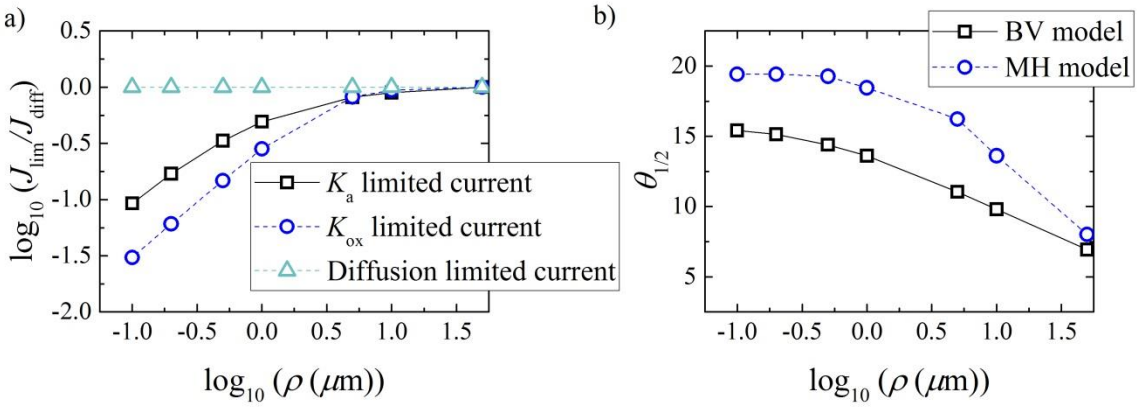


Figure 9 Diffusion effects of the adsorption and the electron transfer limited reactions. a) Normalized limiting current; b) Half-wave potential. The adsorption limited reaction is simulated in the BV model with $K_0 = 10^{-2}$, $K_a = 60$ and $K_{ads} = 1$. The electron transfer limited reaction is simulated in the MH model with $K_0$ = $10^{-2}$, $\lambda^* = 20$, and $K_{ads} = 1$ ($K_a = K_d \gg 1$). The radii of the electrode change from 50.0 $\mu$m to 0.1 $\mu$m. $\theta$ is the dimensionless overpotential for the overall reaction.

## Conclusions

The effects of surface adsorption on Butler-Volmer and Marcus-Hush electron transfer theories have been explored in the context of the Tafel-Volmer mechanism. The voltammetric responses to the change of various kinetic and thermodynamic parameters ($K_0$, $\lambda$, $K_a$, $K_d$, $K_{ads}$) were examined for both BV and MH electron transfer models. When the preceding adsorption step is fast ($K_a$, $K_d \gg 1$), a slow electron transfer step (small $K_0$ and/or small $\lambda^*$) changes the voltammogram of the Tafel-Volmer reaction consistently as it does for a simple unity-stoichiometry, one-electron-transfer reaction.

When the preceding adsorption is taken into consideration as a limiting factor of the overall reaction, different electron transfer kinetics show distinct voltammetric responses, depending on the reversibility of the electron transfer step and kinetic models used to describe the electron transfer step. For an electrochemically reversible Tafel-Volmer reaction ($K_0 \gg 1$), the limiting current can be expressed as a function of the adsorption rate constant $K_a$ while it is independent of the thermodynamics of the adsorption step ($K_{ads}$).

For a non-reversible electron transfer step (relatively small $K_0$), if the electron transfer step is described in terms of the BV model, the limiting current is only dependent on diffusion and the value of $K_a$. But for the MH model, the limiting current is determined by both $K_a$ and $K_{ads}$, especially under weak adsorption conditions (small $K_{ads}$). Therefore, when analysing the voltammograms of a Tafel-Volmer reaction with a weak preceding adsorption step, it is important to consider the kinetic description of the electron transfer in order to correctly understand the mechanism. It is also found that for non-reversible electron transfer, the overpotential changes parabolically with the adsorption equilibrium constant, indicating that both strong and weak adsorption can cause a decrease on the overall reaction rate for the Tafel-Volmer reaction.

This work has also concluded out that the non-diffusion control of the limiting current of steady-state voltammograms is consistent, not only with slow adsorption kinetics, but also with the deviation of the potential variation of the rate constants from the BV formalism. Indeed, the variation of the rate constants with the applied potential predicted by the MH model leads to non-diffusion controlled limiting currents for slow electron transfer kinetics and/or very small electrodes. Such evidence calls for further theoretical and experimental assessment of the kinetics of the Volmer reaction as a possible determining factor of the HOR voltammetry and other similar Tafel-Volmer processes.

## Supporting Information Available

SI section I shows the differences between using surface coverages and fractional surface coverages in the rate equations. SI section II provides the derivation of Eq. (16). SI section III is the derivation of Eq. (36). SI section IV gives the simulation parameters used in Figure 6.

## Acknowledgments

The research is sponsored by the funding from the European Research Council under the European Unions Seventh Framework Programme (FP/2007-2013) / ERC Grant Agreement n. [320403]. EL also thanks the funding received from the European Union Seventh Framework Programme-Marie Curie COFUND (FP7/2007-2013) under UMU Incoming Mobility Programme ACTion (U-IMPACT) Grant Agreement 267143 and by the Fundación Séneca de la Región de Murcia under the III PCTRM 2011-2014 Programme (Project 18968/JLI/13).

## References


1. Batchelor-McAuley, C.; Kätelhön, E.; Barnes, E. O.; Compton, R. G.; Laborda, E.; Molina, A. Recent Advances in Voltammetry. *ChemistryOpen* **2015,** *4*, 224-260.
2. Marcus, R. A. On the Theory of Electron-Transfer Reactions. Vi. Unified Treatment for Homogeneous and Electrode Reactions. *J. Chem. Phys.* **1965,** *43*, 679-701.
3. Hush, N. S. Electron Transfer in Retrospect and Prospect 1: Adiabatic Electrode Processes. *J. Electroanal. Chem.* **1999,** *470*, 170-195.
4. Miller, C.; Graetzel, M. Electrochemistry At .Omega.-Hydroxythiol Coated Electrodes. 2. Measurement of the Density of Electronic States Distributions for Several Outer-Sphere Redox Couples. *J. Phys. Chem.* **1991,** *95*, 5225-5233.
5. Chidsey, C. E. D. Free Energy and Temperature Dependence of Electron Transfer at the Metal-Electrolyte Interface. *Science* **1991,** *251*, 919-922.
6. Chen, S.; Liu, Y. Electrochemistry at Nanometer-Sized Electrodes. *Phys. Chem. Chem. Phys.* **2014,** *16*, 635-652.
7. Feldberg, S. W. Implications of Marcus-Hush Theory for Steady-State Heterogeneous Electron Transfer at an Inlaid Disk Electrode. *Anal. Chem.* **2010,** *82*, 5176-5183.
8. Laborda, E.; Henstridge, M. C.; Batchelor-Mcauley, C.; Compton, R. G. Asymmetric Marcus-Hush Theory for Voltammetry. *Chem. Soc. Rev.* **2013,** *42*, 4894-4905.
9. Bard, A. J. Inner-Sphere Heterogeneous Electrode Reactions. Electrocatalysis and Photocatalysis: The Challenge. *J. Am. Chem. Soc.* **2010,** *132*, 7559-7567.
10. Schmickler, W.; Santos, E. Inner Sphere and Ion-Transfer Reactions. In *Interfacial Electrochemistry*, Springer Berlin Heidelberg: 2010, 10.1007/978-3-642-04937-8_13pp 145-162.
11. Lin, C.; Jiao, X.; Tschulik, K.; Batchelor-McAuley, C.; Compton, R. G. Influence of Adsorption Kinetics Upon the Electrochemically Reversible Hydrogen Oxidation Reaction. *J. Phys. Chem. C* **2015,** *119*, 16121-16130.
12. Frumkin, A. N.; Aikazyan, E. A. Kinetics of Ionization of Molecular Hydrogen on Platinum Electrodes. *Bulletin of the Academy of Sciences of the USSR Division of Chemical Science* **1960,** *8*, 188-197.
13. Vetter, K. J.; Otto, D. *Z.Elektrochem.* **1956,** *60*, 1072-1080.
14. Marcus, R. A. Theory of Electron-Transfer Reaction Rates of Solvated Electrons. *J. Chem. Phys.* **1965,** *43*, 3477-3489.
15. Marcus, R. A. Tutorial on Rate Constants and Reorganization Energies. *J. Electroanal. Chem.* **2000,** *483*, 2-6.
16. Santos, E.; Quaino, P.; Schmickler, W. Theory of Electrocatalysis: Hydrogen Evolution and More. *Phys. Chem. Chem. Phys.* **2012,** *14*, 11224-11233.
17. Santos, E.; Lundin, A.; Pötting, K.; Quaino, P.; Schmickler, W. Model for the Electrocatalysis of Hydrogen Evolution. *Physical Review B* **2009,** *79*, 235436.
18. Guidelli, R.; Compton, R. G.; Feliu, J. M.; Gileadi, E.; Lipkowski, J.; Schmickler, W.; Trasatti, S. Definition of the Transfer Coefficient in Electrochemistry (Iupac Recommendations 2014). *Pure Appl. Chem.* **2014,** *86*, 259-262.
19. Guidelli, R.; Compton, R. G.; Feliu, J. M.; Gileadi, E.; Lipkowski, J.; Schmickler, W.; Trasatti, S. Defining the Transfer Coefficient in Electrochemistry: An Assessment (Iupac Technical Report). *Pure Appl. Chem.* **2014,** *86*, 245-258.
20. Marcus, R. A. Electron Transfer Reactions in Chemistry: Theory and Experiment (Nobel Lecture). *Angewandte Chemie (International Edition in English)* **1993,** *32*, 1111-1121.

21. Marcus, R. A. Chemical and Electrochemical Electron-Transfer Theory. *Annu. Rev. Phys. Chem.* **1964,** *15*, 155-196.
22. Compton, R. G.; Laborda, E.; Ward, K. R. *Understanding Voltammetry: Simulation of Electrode Processes*. Imperial College Press: 2013.
23. Tanner, E. E. L.; Xiong, L.; Barnes, E. O.; Compton, R. G. One Electron Oxygen Reduction in Room Temperature Ionic Liquids: A Comparative Study of Butler–Volmer and Symmetric Marcus–Hush Theories Using Microdisc Electrodes. *J. Electroanal. Chem.* **2014,** *727*, 59-68.
24. Jiao, X.; Batchelor-McAuley, C.; Kätelhön, E.; Ellison, J.; Tschulik, K.; Compton, R. G. The Subtleties of the Reversible Hydrogen Evolution Reaction Arising from the Nonunity Stoichiometry. *J. Phys. Chem. C* **2015,** *119*, 9402-9410.
25. Parsons, R. Volcano Curves in Electrochemistry. In *Catalysis in Electrochemistry*, John Wiley & Sons, Inc.: 2011, 10.1002/9780470929421.ch1pp 1-15.

**Table of Content Graphic**